Mechanistic Studies of Transition Metal-Terephthalate Coordination Complexes upon Electrochemical Lithiation and Delithiation

Hyun Ho Lee, Yuwon Park, Su Hwan Kim, Sun-Hwa Yeon, Sang Kyu Kwak, Kyu Tae Lee, and Sung You Hong**

Dedicated to Professor Reshef Tenne on the occasion of his 70th birthday

Redox-active organic molecules are intriguing candidates as active electrode materials for next-generation rechargeable batteries due to their structural diversity, environmental friendliness, and solution-phase preparation processes. Recently, a transition metal–organic coordination approach is exploited to construct high capacity anodes for lithium-ion rechargeable batteries. Here, a family of transition metal–organic coordination complexes with terephthalate ligands is synthesized that exhibit reversible capacities above 1100 mA h g^{-1}. The reaction mechanism to describe the multi-electron redox processes is investigated at the molecular-level via the synchrotron-sourced X-ray absorption spectroscopy and solid-state NMR analyses. The spectroscopic studies reveal that the electrochemical process involves oxidation state changes of the transition metals followed by additional lithium insertion/extraction in the conjugated aromatic ligands. The combined approaches assisted by synthetic organic chemistry and solid-state analysis provide mechanistic insights into excessive lithiation processes that have implications for the design of high-performance anode materials.

1. Introduction

The harnessing and trapping of renewable energy sources are one of the major hurdles to sustainable development for modern society.[1,2] Strict criteria must be applied to advanced energy storage systems, including pollution-free operating processes, low maintenance costs, and high energy densities, in order to replace nuclear energy or finite supplies of fossil fuels. Lithium-ion battery (LIB) technologies are considered to be promising candidates to meet those demands.[3,4] While most electrode materials in LIBs are based on inorganic elements or compounds, redox-active organic materials have recently gained attention as a fascinating class due to their eco-friendly production starting from renewable resources (biomass or natural compounds) and solution-phase reactions that avoid high-energy ceramic processes.[5–9] Moreover, the structural diversity of the organic building blocks (as scaffolds and substituents) allows the rational design of high-performance electrode materials.[10–12] The Chen group proposed a molecular-level engineering strategy to improve cell performance with respect to working potential, power density, rate capability, and cycling stability through the incorporation of fused heterocyclic moieties and pre-aromatic 1,2-dicarbonyl functional groups.[13,14]

Ever since the first demonstration of a primary battery utilizing organic molecules by Williams et al. in 1969,[15] new classes of organic materials have been developed for secondary batteries; these include conducting polymers, nitroxide-bearing radical polymers, disulfides, and quinone derivatives.[16–19] In 2009, the seminal work of Tarascon and co-workers introduced organic anode materials on the basis of conjugated dicarboxylates including dilithium terephthalate (Li_2TP) and dilithium *trans,trans*-muconate.[20] The organic salts exhibited excellent electrochemical performance in terms of enhanced thermal stability, good cyclability, and suitable redox potential. As shown in **Scheme 1**a, Li_2TP reacts with two lithium atoms to afford a conjugated enolate with a reversible capacity of about 300 mA h g^{-1}. According to Hünig's classification, the carboxylate-enolate interconversion of Li_2TP belongs to an inverse-Wurster-type system, where carboxylates are located outside a cyclic π-system that has aromaticity in the oxidized state.[21] Despite noteworthy progress, the utilization of organic-based materials involving two-electron insertion process is practically limited due to relatively low specific capacity values.

H. H. Lee, S. H. Kim, Prof. S. K. Kwak, Prof. S. Y. Hong
School of Energy and Chemical Engineering
Ulsan National Institute of Science and Technology (UNIST)
KIER-UNIST Advanced Center for Energy
Ulsan 689-798, Republic of Korea
E-mail: syhong@unist.ac.kr

Dr. Y. Park, Prof. K. T. Lee
Department of Chemical and Biological Engineering
Seoul National University
599 Gwanangno, Gwanak-gu, Seoul 515-742, Republic of Korea
E-mail: ktlee@snu.ac.kr

Dr. S.-H. Yeon
Korea Institute of Energy Research (KIER)
152 Gajeong-ro, Yuseong-gu, Daejeon 305-343, Republic of Korea

DOI: 10.1002/adfm.201501436

© 2015 WILEY-VCH Verlag GmbH & Co. KGaA, Weinheim

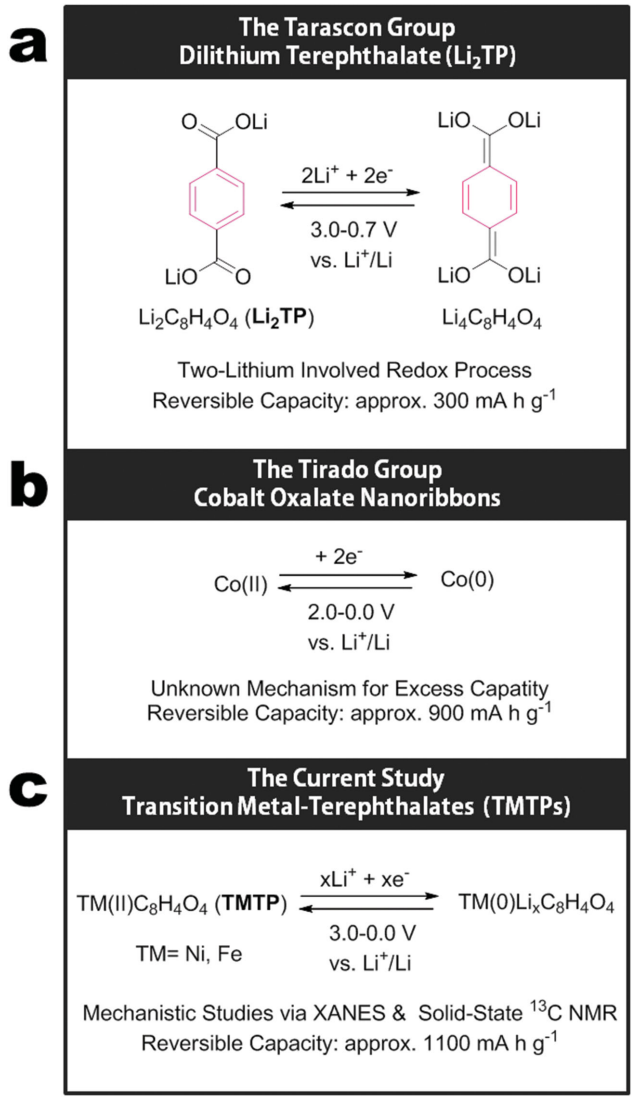

Scheme 1. Electrochemical lithiation and delithiation of a) dilithium terephthalate, b) cobalt oxalate nanoribbons, and c) transition metal-terephthalates.

In 2012, Han et al. demonstrated fused aromatic molecules bearing anhydride functional groups can accommodate lithium ions forming up to 1:1 Li/C complex corresponding to theoretical capacity of ca. 2000 mA h g^{-1}.[22] Later, we reported the excessive lithiation behaviors even in non-fused (hetero)aromatics with dicarboxylates.[23] However, these systems require precycles to reach the maximum reversible capacities. In addition, Li_2TP electrode displays significant capacity loss since excessively lithiated compounds containing highly polar C—Li bonds can react with electrolytes. To attain high-capacity anode materials with stable cycle performance, the transition metal–organic complexation approach has been exploited to extend the range of organic-based active materials.[24] The first row transition metal–carboxylate complexes have been utilized for LIBs, taking advantage of their metal–ligand coordination bond stability. For example, a lithium- and nickel-1,4,5,8-naphthalenetetracarboxylate composite displayed a reversible capacity of ca. 482 mA h g^{-1}.[25] A nanostructured cobalt oxalate (Scheme 1b) delivered even higher reversible capacity, approaching 900 mA h g^{-1}, which involved the redox processes of Co(II)/Co(0).[26] Yet, the fundamental understanding of the reaction mechanism of coordination complexes remains unsolved due to the experimental challenges in identifying the exact redox sites (transition metal ions/organic ligands) and multi-electron involved redox mechanism. Here, we report the synthesis of a family of transition metal–terephthalate complexes (TMTPs) with reversible capacities above 1100 mA h g^{-1} at 30 mA g^{-1}, which are the highest values among organic-based coordination compounds to date (Scheme 1c). X-ray absorption spectroscopy and solid-state cross-polarization magic-angle-spinning (CP/MAS) NMR techniques were applied to elucidate the molecular transformations during the electrochemical lithiation and delithiation processes.

2. Results and Discussion

2.1. Synthesis and Characterization of TMTPs

A family of transition metal–organic complexes was prepared through salt metathesis reactions between divalent transition metal ions and a terephthalate precursor (disodium terephthalate, Na_2TP) according to previously reported methods (**Scheme 2**, see also Supporting Information).[27] In aqueous solution, the divalent metal salts reacted to form the TMTP complexes, which preferentially precipitated. The prolonged heating of reaction mixtures afforded hydroxo ligand-containing coordination complexes (basic coordination complexes);[28] this phenomenon is attributed to the partial deprotonation of the aqua ligand.

As shown in **Figure 1**, the Fourier-transform infrared (FTIR) spectrum of nickel terephthalate (NiTP) tetrahydrate showed asymmetric and symmetric stretching bands at 1537 and 1386 cm^{-1}, with complete absence of the initial bands from Na_2TP at 1550 and 1382 cm^{-1} assigned to ν_{as}(COONa) and ν_s(COONa), respectively. Noticeably, the IR bands in the basic NiTP monohydrate were shifted to 1565 and 1373 cm^{-1}, showing a large difference in the asymmetric stretching mode compared to $NiTP \cdot 4H_2O$. The basic $NiTP \cdot H_2O$ also presented narrow and broad bands at 3579 and 3401 cm^{-1} corresponding to hydroxo and aqua ligands, respectively. The iron terephthalate $(FeTP) \cdot 2H_2O$ exhibited strong IR bands at

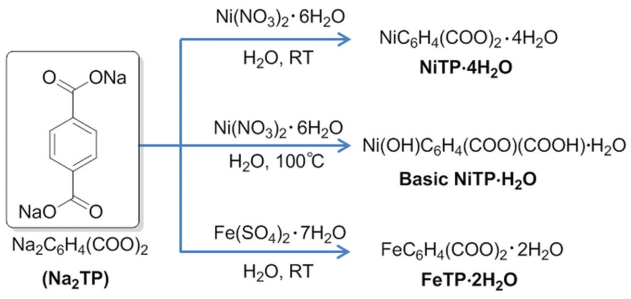

Scheme 2. Preparation of transition metal-terephthalate (TMTP) complexes.

© 2015 WILEY-VCH Verlag GmbH & Co. KGaA, Weinheim

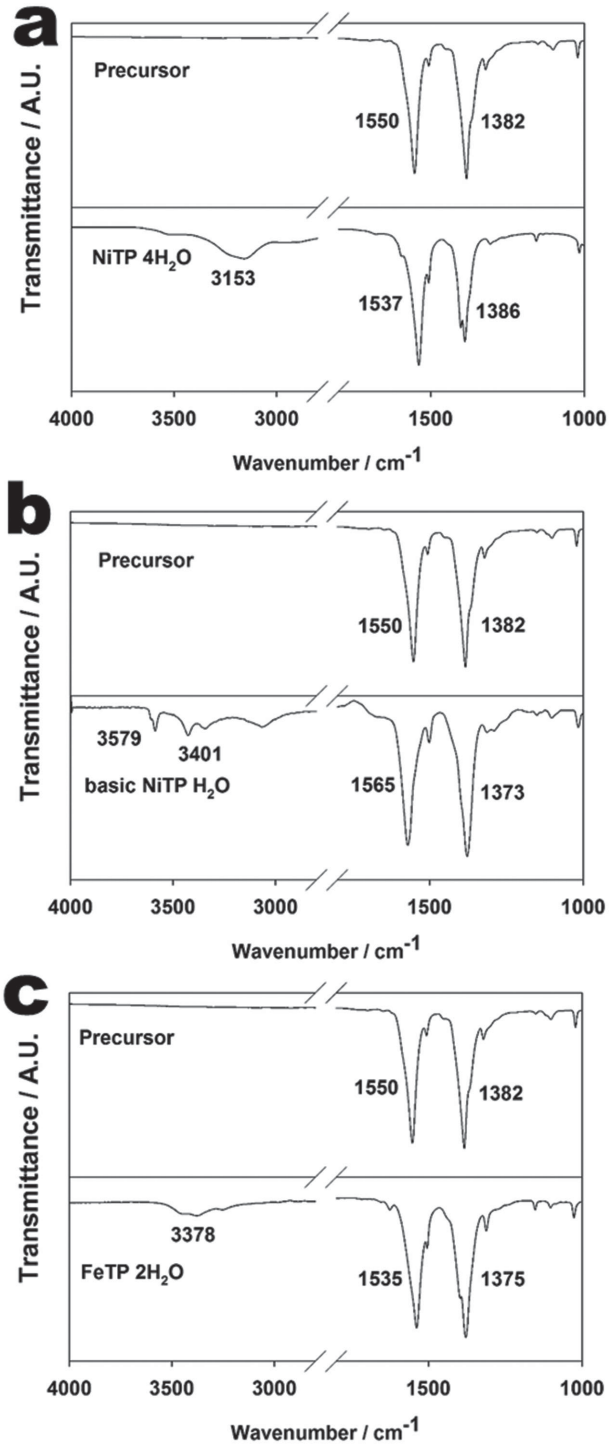

Figure 1. FTIR spectra of a) NiTP tetrahydrate, b) basic NiTP monohydrate, and c) FeTP dihydrate.

1535 and 1375 cm^{-1}, assigned to ν_{as}(COOFe) and ν_{s}(COOFe), respectively.

Thermogravimetric and differential thermal analyses (TGA/DTA) were performed to investigate the hydration states and thermal stabilities of TMTPs, as shown in **Figure 2**a–c. The onset of weight loss from the NiTP·$4H_2O$ started at 135 °C, with a magnitude of about 22% from the initial weight, confirming the four aqua ligands. Subsequent weight loss associated with decomposition of the complex was observed at 425 °C and indicated its robust thermal stability. Basic NiTP·H_2O underwent dehydration at 135 °C with the loss of a single water molecule, with subsequent weight losses at 315 °C and 427 °C ascribed to the decomposition of carboxylic acids and carboxylates. The dehydration of FeTP·$2H_2O$ occurred at 151 °C, with 13.8% weight loss attributed to the dihydrate. The FeTP complex decomposed at 481 °C, indicating its stronger thermal stability compared with the nickel–organic complexes. Since lithium reacts violently with water to form lithium hydroxide, lithium hydride, and Li_2O attributed to irreversible capacities,[29] the hydrates were annealed prior to assembly of the electrochemical cells. As deduced by the TGA curves, the TMTP samples annealed at 150 °C for 10 h under vacuum manifested complete dehydration. The formations of TMTP hydrates were further determined by X-ray diffraction (XRD) patterns and the crystal structures of as-prepared samples were well matched with previous reports (see Figure 2d–f).[27,28] After annealing, disordered structures of the dehydrated TMTPs were observed in the XRD patterns. Unlike NiTP·$4H_2O$ and FeTP·$2H_2O$, basic NiTP·H_2O revealed minimal structural changes due to its low hydration state.

2.2. Electrochemical Studies of TMTPs

The electrochemical performance of the pre-annealed TMTP electrodes was evaluated by galvanostatic cycling. **Figure 3**a–c shows the charge/discharge profiles of the anhydrous coordination complexes NiTP, basic NiTP, and FeTP in Li cells at a current density of 30 mA g^{-1}. It is noteworthy that NiTP and basic NiTP present nearly identical voltage profiles. Initially, their electrode potentials drop abruptly to a first plateau at 1.38 V vs. Li^+/Li, and then, they decay gradually below about 1.0 V vs. Li^+/Li while delivering high capacity. FeTP electrode also shows similar electrochemical behavior. The large irreversible capacities of the anhydrous TMTPs during the first discharge (lithiation) are ascribed to the contribution from the formation of a solid electrolyte interphase (SEI) resulting in low Coulombic efficiencies (≈79% for NiTP, ≈78% for basic NiTP, and ≈68% for FeTP). However, the Li_xNiTP/Li and Li_xFeTP/Li cells showed improved Coulombic efficiencies—close to 99%—after five cycles (see Figure S1a, Supporting Information). Reversible capacities were maintained at 1402 mA h g^{-1} for NiTP, 1474 mA h g^{-1} for basic NiTP, and 1474 mA h g^{-1} for FeTP (Figure 3d). Due to the low electric conductivities of the organic-based complexes, 37.5 wt% conductive carbon (Super P) was included. Even after subtraction of the maximum capacity (293 mA h g^{-1}) delivered from the Super P,[23] the remaining capacities of the NiTP, basic NiTP, and FeTP electrodes still reached 1109, 1181, and 1181 mA h g^{-1}, respectively, corresponding to about 10 lithium-insertion processes (Figure S1b, Supporting Information). In addition, the rate performance of the TMTPs was investigated (Figure 3e). The transition metal–organic complexes delivered about 63%–65% of their original capacities even at 500 mA g^{-1}. XRD patterns of TMTP cells displayed progressive amorphization process during the initial lithiation

© 2015 WILEY-VCH Verlag GmbH & Co. KGaA, Weinheim

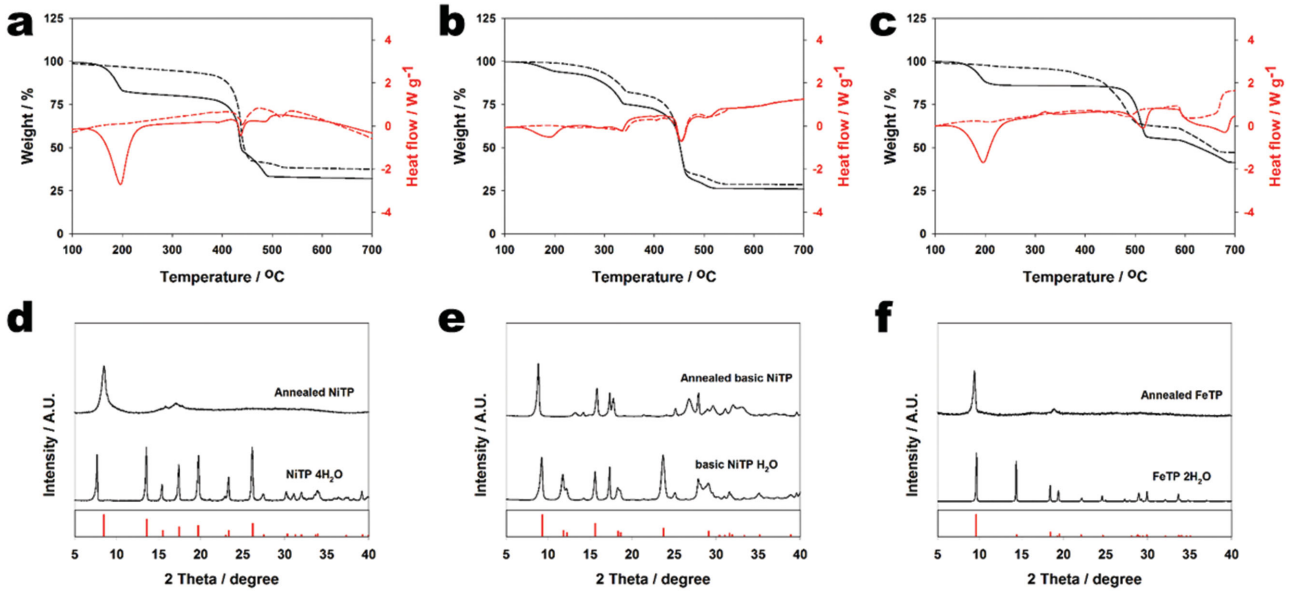

Figure 2. Characterization of the TMTPs. a–c) TGA(black)/DTA(red) of NiTP, basic NiTP, and FeTP, respectively before (the solid line) and after (the dotted line) annealing; d–f) XRD powder patterns of NiTP, basic NiTP, and FeTP, respectively.

discharge cycle (Figure S2–3, Supporting Information), which is ascribed to the loss of long-range order of molecular packing.

2.3. XANES Studies of (basic) NiTP electrodes

After achieving high electrochemical performance, our attention was shifted to the investigation of the origin of the high capacities in the TMTPs. To determine the redox sites of the transition metal complexes associated with the excessive lithiation, we monitored the oxidation states of the transition metals via X-ray absorption near-edge structure (XANES) spectroscopy, where the near-edge spectra reveal element-specific characteristics depending on the oxidation state.[30] As shown in **Figure 4**, the normalized Ni K-edge XANES data for NiTP were collected at various

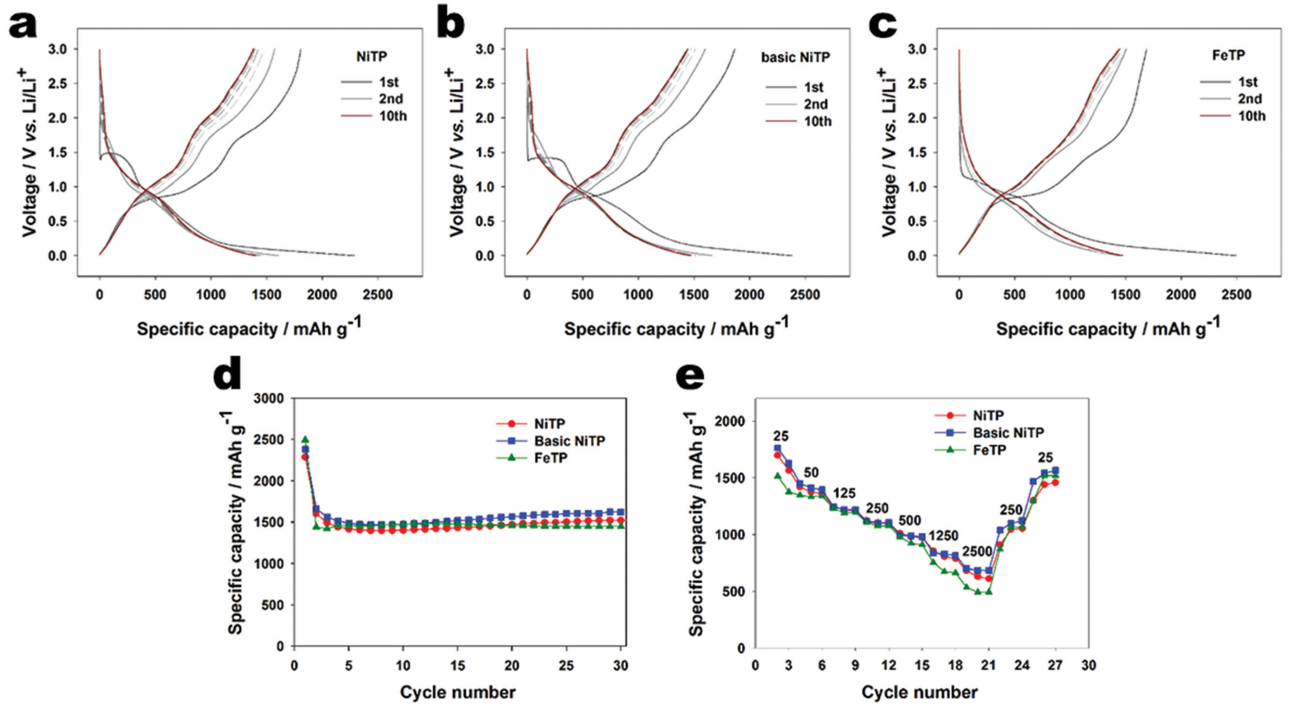

Figure 3. Electrochemical performance. a–c) Voltage profiles of anhydrous NiTP, basic NiTP, and FeTP, respectively, d) cyclability of the TMTPs at a current density of 30 mA g^{-1}, e) rate performances of the TMTPs.

© 2015 WILEY-VCH Verlag GmbH & Co. KGaA, Weinheim

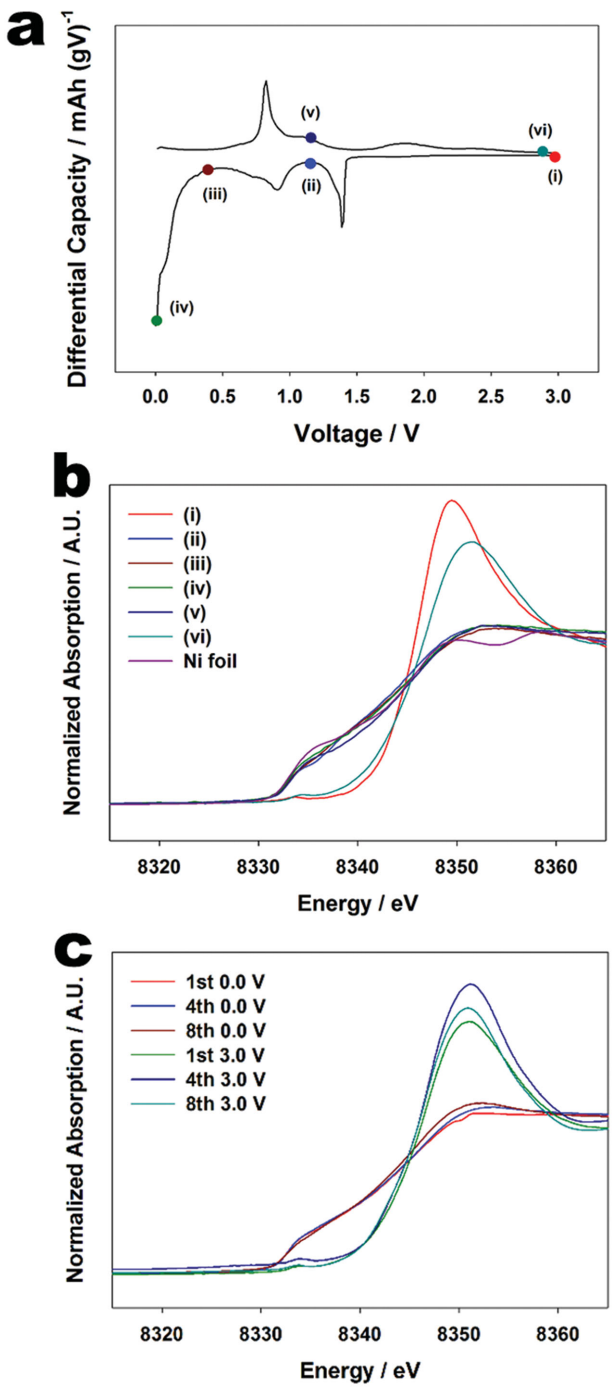

Figure 4. a) dQ/dV for the first cycle of anydrous NiTP, b) Ni K-edge XANES spectra of anhydrous NiTP electrodes during the first cycle, c) Ni K-edge XANES spectra of anhydrous NiTP electrodes during the first, fourth, and eighth cycle.

points during the first cycle on the basis of the differential capacity (dQ/dV), having reductive peaks at 1.38 and 0.87 V as well as oxidative peaks at 0.82 and 1.85 V. Notably, basic NiTP showed almost identical spectra (Figure S4, Supporting Information). Initially, NiTP showed a weak pre-edge peak at 8333.4 eV assigned to the $1s \rightarrow 3d$ transition, which can arise from electric quadruple coupling or $4p$–$3d$ orbital mixing.[31] A strong white line appeared with an inflection point at 8340.6 eV. During the first discharge until the redox potential reaches 1.1 V, the lithiation of NiTP was demonstrated by the absorption edge shift to lower energy, near that of Ni foil, revealing the reduction of Ni(II) to Ni(0) (Equation (1), Stage I). No dramatic changes were observed during prolonged lithiation until the redox potential reached 0.0 V. Upon the initial extraction of lithium until the redox potential reached 1.1 V, no marked changes were found. When the electrode was further delithiated up to 3.0 V, the initial NiTP phase was recovered. However, a smaller and shifted (+0.8 eV) main edge was observed. Since XANES spectral features are sensitive to geometrical structures, the peak shapes and positions can be influenced by changes in local structural environments.[30,31] As shown in Figure S2 (Supporting Information), NiTP electrode undergoes progressive amorphization during the electrochemical processes. The higher disorder caused by amorphization can result in the slight distortions in the strong white lines as demonstrated by other groups showing relatively flatter or smaller lines with slight peak shifts.[32,33] The restriction of the valence changes of the NiTPs to two electron transfers (ca. 240 mA h g^{-1}), however, cannot fully explain the origin of the high capacities above 1100 mA h g^{-1}.

$$Ni(II)C_8H_4O_4 + 2(Li^+ + e^-) \rightleftarrows Ni(0) + Li_2C_8H_4O_4 \quad (1)$$

2.4. Solid-State ^{13}C NMR Studies of Basic NiTPs electrodes

In order to clarify the additional redox sites in the coordination complexes, molecular structure transformations of the organic ligand were traced via NMR spectroscopic studies (**Figure 5**). Since NMR techniques use the magnetic properties of the nucleus, they can detect detailed local information about the molecular structure with respect to chemical bonds, the electronic environment of the nucleus, and the proximity of neighboring atoms.[34] Despite high sensitivity of solution-state NMR spectroscopy, solid-state NMR analysis was selected for two reasons. First of all, it is a more suitable method to clearly describe solid-state processes of electrochemical lithiation. Second, it can reduce potential artifacts related with the chemical reactions between NMR solvents and highly lithiated electrode materials. To achieve high-resolution solid-state NMR spectra, CP/MAS techniques and a stable isotopic labeling method were combined. Since the naturally abundant (98.9%) carbon-12 atom is NMR-inactive, ^{13}C labeled basic nickel terephthalate (basic NiTP-$^{13}C_2$) was prepared (Figure 5b), where two carboxylate carbons were enriched with carbon-13 for the selective enhancement of the signals from solid-state CP/MAS ^{13}C NMR spectroscopy with the chemical shift of 174.9 ppm unlike conventional nonlabeled samples. The carbon-13 bearing molecule was monitored during the electrochemical processes to examine carboxylate transformations (see Figure 5a). The labeled sample exhibited a resonance line at 174.9 ppm. When the electrode was discharged to 1.1 V for the initial lithiation, no significant changes in the NMR pattern appeared, although transition metal reduction was detected by XANES analysis (Stage I). Once the cell potential reached

© 2015 WILEY-VCH Verlag GmbH & Co. KGaA, Weinheim

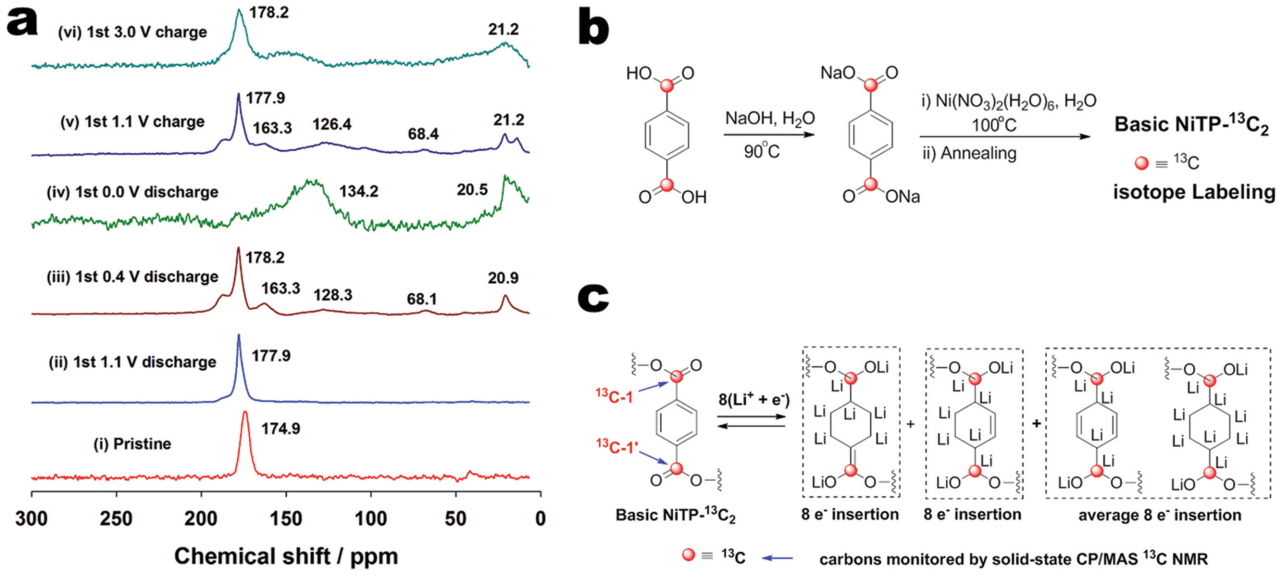

Figure 5. a) Solid-state CP/MAS ^{13}C NMR spectra of C-13 labeled basic-NiTP (basic NiTP-$^{13}C_2$), b) Preparation of isotope-labeled basic NiTP-$^{13}C_2$, c) Schematic representation of excessive lithiation on basic NiTP-$^{13}C_2$.

0.4 V, a new peak at about 163 ppm ascribed to the highly conjugated enolate was observed. After pursuing further lithiation to 0.0 V, two broad resonance bands started to evolve in the lower frequency region centered at about 134.2 and 20.5 ppm, assigned to more saturated structures (see Figure S5, Supporting Information). During the discharge cycle, the starting material (basic NiTP-$^{13}C_2$) loses aromaticity and the degree of unsaturation decreases. Since electrochemically lithiated products have more saturated structures, they have reduced ring-current effect and also possess higher electron densities in their organic scaffolds. Thereby, the chemical shifts move towards more shielded region. Previously, Han et al. reported the changes of chemical shifts of a fused cyclic compound to the more shielded region during a discharge cycle.[22] In addition, lithium enolates with less conjugated structures are also observed in the lower frequency region.[35,36] It is noteworthy that labeled ^{13}C-1 and ^{13}C-1' are solely detected as shown in Figure 5c. Whereas ^{1}H NMR spectroscopy allows quantitative analysis via peak integration, ^{13}C NMR technique is a qualitative analytic method identifying molecular structures. Terephthalate reduction does not stop at the enolate stage (ca. 163 ppm), which is ascribed to two-lithium insertion.[20] Terephthalate ligand is further lithiated to afford more saturated organic scaffolds (134.2 and 20.5 ppm), highlighting the major role of the organic ligand as a multiple redox site (Equation (2), Stage II), which is consistent with voltage profiles delivering high capacities below 1.0 V (Figure 3a–c). During the subsequent delithiation, the carbonyl signal at 178.2 ppm was recovered, indicating the electrochemical reversibility of the lithiation/delithiation processes.

$$Ni(0) + Li_2C_8H_4O_4 + (x\text{-}2)Li^+ + (x\text{-}2)e^- \rightleftarrows Ni(0) + Li_xC_8H_4O_4 \quad (2)$$

On the basis of the combined XANES and NMR spectroscopic studies, a two-stage mechanism was proposed that accounts for the excessive lithiation of TMTPs (**Scheme 3**): divalent transition metal ion reduction followed by successive lithiation of the organic terephthalate ligands to generate more saturated organic scaffolds. The superior electrochemical performances of anhydrous TMTP are presumably originated via the elemental transition metal formation. The homogenous elemental transition nanoparticle formations were observed in amorphous Li_2TP matrix (see Figure S6, Supporting Information). The conversion-type electrode materials often exhibit excellent electrochemical performances due to enhanced electrochemical surface reactivity originated from transition metal nanoparticles (size less than 5 nm).[37,38] In addition, SEM cross-sectional analyses of Li_xNiTP/Li electrodes revealed morphological changes during electrochemical cycles (Figure S7, Supporting Information). A large number of porous cavities with diverse shapes were observed for pristine NiTP electrode. As the lithiation process goes on, however, most of pores are collapsed minimizing volume changes behaving as buffer spaces.

3. Conclusion

In summary, a family of transition metal–organic coordination complexes was synthesized as anode materials via salt metathesis. The compounds exhibited superior electrochemical performance with high capacities and good cyclability. To identify the electrochemical lithiation mechanism of the coordination complexes, combined XANES and solid-state ^{13}C NMR spectroscopic studies were performed. They revealed that lithiation occurs through the electrochemical processes involving transition metal reduction and subsequent excessive lithiation of the organic ligands. In particular, CP/MAS NMR techniques combined with ^{13}C isotope labeling showed the change of resonant frequency during electrochemical lithiation and delithiation. We expect that the current approach using transition metal–organic complexation and solid-state analysis will

© 2015 WILEY-VCH Verlag GmbH & Co. KGaA, Weinheim

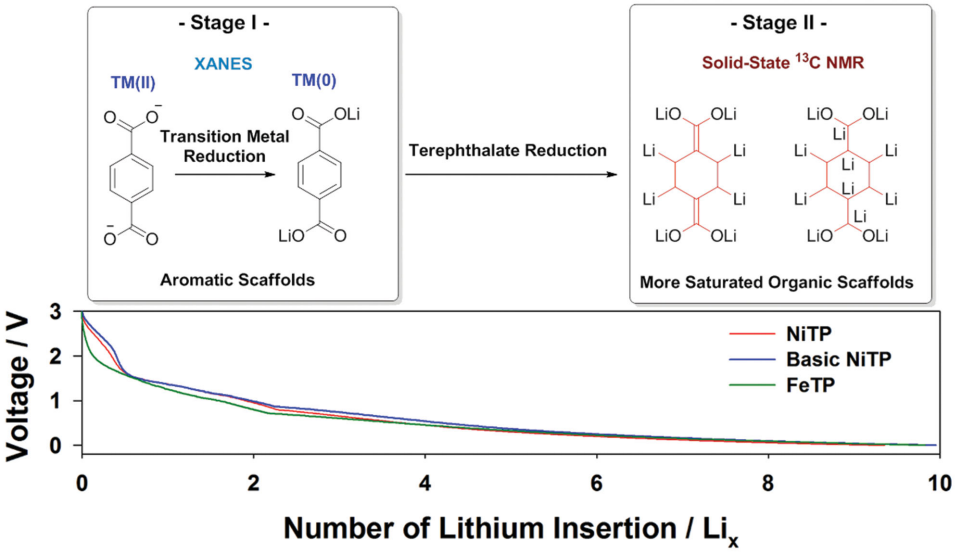

Scheme 3. Proposed reaction mechanism of anhydrous TMTPs upon the electrochemical lithiation.

provide an important step toward the development of improved high-performance anode materials for LIBs.

4. Experimental Section

Characterization: XANES data were recorded using the 7D beam line at the Pohang Light Source (Pohang, Korea). The data were measured in transmission mode using gas-filled ionization chambers as detectors. Electrochemical cells were disassembled and the collected powder was loaded into a probe in an argon-filled glove box. Solid-state CP/MAS ^{13}C NMR spectra were recorded on a Varian 600 spectrometer at a spin rate of 35 kHz with a 1.6 mm Agilent Fast MAS probe. Chemical shifts are given in the δ-scale in ppm. FTIR spectra were measured on a Nicolet FT-IR 200 (ATR, Thermo Scientific). Absorption bands were recorded in wavenumbers (cm^{-1}). Thermal analysis was performed at a heating rate of 10 °C per min under nitrogen atmosphere using a TA Instruments Q600 thermogravimetric analyzer. XRD data were collected on a Rigaku D/MAX2500V/PC powder diffractometer using Cu Kα radiation (λ = 1.5405 Å). Scanning electron microscopy (SEM) samples were examined in a Nano 230 field-emission SEM (FE-SEM) instrument.

Synthesis: Solvents and reagents were obtained from standard suppliers. Transition metal-coordination complexes were synthesized according to previously reported salt metathesis reactions.[27,28] As-prepared coordination complexes were annealed at 150 °C for 10 h before coin cell assembly. The detailed procedures were described in the Supporting Information.

Electrochemical Characterization: Samples of electrochemically active materials were mixed with carbon black (Super P) and carboxymethyl cellulose (CMC) in a 4:3:1 weight ratio. The electrochemical performance was evaluated using 2032 coin cells with a lithium metal anode and 0.8 M $LiPF_6$ in ethylene carbonate and diethyl carbonate (1:1 v/v) electrolyte solution. Galvanostatic experiments were performed at a current density of 30 mA g^{-1} at 25 °C.

Supporting Information

Supporting Information is available from the Wiley Online Library or from the author.

Acknowledgements

This work was supported by the National Research Foundation of Korea (NRF) Grant (NRF-2013R1A1A2060695), the Korea Institute of Energy Research Grant (KIER)(B5-2422), the Energy Efficiency & Resources of the Korea Institute of Energy Technology Evaluation and Planning Grant (Project no. 20112010100140), and the Industrial Strategic Technology Development Program (Project No. 10050477, Development of separator with low thermal shrinkage and electrolyte with high ionic conductivity for Na-ion batteries) of Ministry of Trade, Industry & Energy (Republic of Korea). The authors are grateful to Prof. Yoon Seok Jung for helpful discussions.

Received: April 10, 2015
Revised: June 8, 2015
Published online: July 2, 2015

[1] J.-M. Tarascon, *Phil. Trans. R. Soc. A* **2010**, *368*, 3227.
[2] J. B. Goodenough, *Energy Environ. Sci.* **2014**, *7*, 14.
[3] B. Dunn, H. Kamath, J.-M. Tarascon, *Science* **2011**, *334*, 928.
[4] D. Larcher, J.-M.Tarascon, *Nat. Chem.* **2015**, *7*, 19.
[5] H. Chen, M. Armand, G. Demailly, F. Dolhem, P. Poizot, J. M. Tarascon, *ChemSusChem* **2008**, *1*, 348.
[6] H. Chen, M. Armand, M. Courty, M. Jiang, C. P. Grey, F. Dolhem, J.-M. Tarascon, P. Poizot, *J. Am. Chem. Soc.* **2009**, *131*, 8984.
[7] W. Walker, S. Grugeon, O. Mentre, S. Laruelle, J.-M. Tarascon, F. Wudl, *J. Am. Chem. Soc.* **2010**, *132*, 6517.
[8] a) M. Lee, J. Hong, D. H. Seo, D. H. Nam, K. T. Nam, K. Kang, C. B. Park, *Angew. Chem. Int. Ed.* **2013**, *52*, 8322; b) M. Lee, J. Hong, D. H. Seo, D. H. Nam, K. T. Nam, K. Kang, C. B. Park, *Angew. Chem.* **2013**, *125*, 8480.
[9] H. Wu, S. A. Shevlin, Q. Meng, W. Guo, Y. Meng, K. Lu, Z. Wei, Z. Guo, *Adv. Mater.* **2014**, *26*, 3338.
[10] Y. Park, D.-S. Shin, S. H. Woo, N. S. Choi, K. H. Shin, S. M. Oh, K. T. Lee, S. Y. Hong, *Adv. Mater.* **2012**, *24*, 3562.
[11] Z. Song, H. Zhou, *Energy Environ. Sci.* **2013**, *6*, 2280.
[12] S. Y. Hong, Y. Kim, Y. Park, A. Choi, N. S. Choi, K. T. Lee, *Energy Environ. Sci.* **2013**, *6*, 2067.
[13] Y. Liang, P. Zhang, J. Chen, *Chem. Sci.* **2013**, *4*, 1330.

© 2015 WILEY-VCH Verlag GmbH & Co. KGaA, Weinheim

[14] Y. Liang, P. Zhang, S. Yang, Z. Tao, J. Chen, *Adv. Energy Mater.* **2013**, *3*, 600.
[15] D. L. Williams, J. J. Byrned, J. S. Driscoll, *J. Electrochem. Soc.* **1969**, *116*, 2.
[16] P. Poizot, F. Dolhem, *Energy Environ. Sci.* **2011**, *4*, 2003.
[17] Y. Liang, Z. Tao, J. Chen, *Adv. Energy Mater.* **2012**, *2*, 742.
[18] T. Nokami, T. Matsuo, Y. Inatomi, N. Hojo, T. Tsukagoshi, H. Yoshizawa, A. Shimizu, H. Kuramoto, K. Komae, H. Tsuyama, J.-I. Yoshida, *J. Am. Chem. Soc.* **2012**, *134*, 19694.
[19] S. Gottis, A.-L. Barres, F. Dolhem, P. Poizot, *ACS Appl. Mater. Interfaces* **2014**, *6*, 10870.
[20] M. Armand, S. Grugeon, H. Vezin, S. Laruelle, P. Ribiere, P. Poizot, J.-M. Tarascon, *Nat. Mater.* **2009**, *8*, 120.
[21] a) K. Deuchert, S. Hünig, *Angew. Chem. Int. Ed.* **1978**, *17*, 875; b) K. Deuchert, S. Hünig, *Angew. Chem.* **1978**, *90*, 927.
[22] a) X. Han, G. Qing, J. Sun, T. Sun, *Angew. Chem. Int. Ed.* **2012**, *51*, 5147; b) X. Han, G. Qing, J. Sun, T. Sun, *Angew. Chem.* **2012**, *124*, 5237.
[23] H. H. Lee, Y. Park, K. H. Shin, K. T. Lee, S. Y. Hong, *ACS Appl. Mater. Interfaces* **2014**, *6*, 19118.
[24] B. Guo, Q. Kong, Y. Zhu, Z. Wang, M. Wan, L. Chen, *Chem. Eur. J.* **2011**, *17*, 14878.
[25] X. Han, F. Yi, T. Sun, J. Sun, *Electrochem. Commun.* **2012**, *25*, 136.
[26] M. J. Aragón, B. León, C. Pérez Vicente, J. L. Tirado, A. V. Chadwick, A. Berko, S.-Y. Beh, *Chem. Mater.* **2009**, *21*, 1834.
[27] J. A. Kaduk, *Acta Crystallogr., Sect. B* **2002**, *58*, 815.
[28] F. J. Sherif, *Ind. Eng. Chem. Prod. Res. Dev.* **1970**, *9*, 408.
[29] D. Aurbach, I. Weissman, *Electrochem. Commun.* **1999**, *1*, 324.
[30] G. Bunker, *Introduction to XAFS*, Cambridge University Press, Cambridge, UK **2010**.
[31] K. I. Pandya, R. W. Hoffman, J. McBreen, W. E. O'Grady, *J. Electrochem. Soc.* **1990**, *137*, 383.
[32] M. Backman, F. Djurabekova, O. H. Pakarinen, K. Nordlund, L. L. Araujo, M. C. Ridgway, *Phys. Rev. B* **2009**, *80*, 144109.
[33] S. J. Park, M. H. Jang, S. J. Park, M. Ahn, D. B. Park, D.-H. Ko, M.-H. Cho, *J. Mater. Chem.* **2012**, *22*, 16527.
[34] N. E. Jacobsen, *NMR Spectroscopy Explained*, John Wiley & Sons, Ltd., New Jersey, USA **2007**.
[35] H. O. House, A. V. Prabhu, W. V. Phillips, *J. Org. Chem.* **1976**, *41*, 1209.
[36] G. W. Spears, C. E. Caufield, W. C. Still, *J. Org. Chem.* **1987**, *52*, 1226.
[37] P. Poizot, S. Laruelle, S. Grugeon, L. Dupont, J.-M. Tarascon, *Nature* **2000**, *407*, 496.
[38] Z.-W. Fu, Y. Wang, X.-L. Yue, S.-L. Zhao, Q.-Z. Qin, *J. Phys. Chem. B* **2004**, *108*, 2236.

© 2015 WILEY-VCH Verlag GmbH & Co. KGaA, Weinheim